

Supplemental Material

An absolutely dated record of climate change over the last three glacial–interglacial cycles from Chinese loess deposits

CONTENTS

- (1) Luminescence dating studies on the Chinese Loess Plateau
- (2) Details of the sampling and experiments
- (3) Tests of the reliability of the dating protocols
- (4) Global climate evidence for reassigning the age of the MIS 8/9 boundary to ca. 280 ka

LIST OF TABLES AND FIGURES

- Table S1. The SAR MET-pIRIR dating protocol used in this study
- Table S2. The MAR MET-pIRIR dating protocol used in this study
- Table S3. Boundary ages from orbitally-tuned timescales and the luminescence age model
- Figure S1: SAR D_e estimation from the dose response curves
- Figure S2. Comparison of SAR and MAR D_e values versus sampling depth
- Figure S3. Standardized growth curves (SGCs) constructed for the MAR protocol
- Figure S4. Dose rates and ages for samples at the S1/L2 boundary
- Figure S5. Residual doses after solar bleaching
- Figure S6. SAR D_e values at different stimulation temperatures
- Figure S7. Dose recovery results with two different test doses (T_d)

REFERENCES

(1) Luminescence dating studies on the Chinese Loess Plateau

The single-aliquot regenerative-dose (SAR) protocol has greatly improved the precision and accuracy of the optically stimulated luminescence (OSL) dating of quartz (Murray and Wintle, 2000; Wintle and Murray, 2006), and it has been widely applied to constrain the chronology of the loess–paleosol sequences of the Chinese Loess Plateau (CLP). These quartz OSL–dated sites include, but are not limited to, the following sections: Luochuan (Buylaert et al., 2007; Lu et al., 2007; Lai, 2010; Chapot et al., 2012; Fu et al., 2012; Lu et al., 2013), Weinan (Kang et al., 2013, 2018, 2020), Xifeng (Lu et al., 2006; Stevens et al., 2006, 2007; Timar-Gabor et al., 2017), Huanxian (Lu et al., 2006), Beiguoyuan (Stevens et al., 2006, 2007, 2008, 2013), Xunyi (Stevens et al., 2008; Lu et al., 2013), Yuanbao (Lai and Wintle 2006; Lai et al., 2007), Lingtai (Peric et al., 2019), Zhongjiacai (Buylaert et al., 2008), Jingyuan (Sun et al., 2010, 2012), Gulang (Sun et al., 2012), Yulin (Lu et al., 2013), Jingbian (Stevens et al., 2018), and Zhenbeitai (Wu et al., 2019).

Among these studies, several have proposed the general continuity of dust accumulation on millennial timescales, such as during the last glaciation at the Jingyuan section (Sun et al., 2010), and during Marine Isotope Stage (MIS) 2 at multiple sections (Kang et al., 2015). Meanwhile, several studies identified age gaps of 4–5 kyr or ~10 kyr at sections such as Xifeng, Huanxian, Beiguoyuan and Tuxiangdao (Lu et al., 2006; Stevens et al., 2006; Buylaert et al., 2008).

As the quartz OSL signal saturates at a relatively low dose, generally it cannot provide reliable ages beyond 100 ka, and thus OSL dating applications on the CLP are mainly restricted

to the Holocene and last glacial periods (S0 and Li units). Underestimation of quartz OSL ages on the CLP appeared from 70 ka (Lai, 2010) or even 40 ka (Buylaert et al., 2007; Chapot et al., 2012; Timar-Gabor et al., 2017; Peric et al., 2019), which is much younger than expected from the shape of the dose response curve (DRC). The early appearance of age underestimation may be related to the anomalously low signal stability of quartz on the CLP (Fan et al., 2011; Lai and Fan, 2014), and the deviation between the natural and laboratory DRCs: i.e., the natural DRC reaches saturation much earlier (Timar-Gabor and Wintle, 2013; Timar-Gabor et al., 2015). The thermal-transferred OSL (TT-OSL) of quartz continues to grow at very high doses and has shown the potential for dating as far back as the Brunhes/Matuyama (B/M) boundary at ~780 ka, by applying pulsed irradiation for DRC construction (Wang et al., 2006). Using TT-OSL dating, Kang et al. (2011) dated the last interglacial palaeosol (unit S1) at the Weinan section. However, TT-OSL dating has not been widely applied on the CLP, probably due to the low thermal stability (Chapot et al., 2016; Liu et al., 2016). The violet stimulated luminescence (VSL) of quartz also has a very high characteristic saturation dose (D_0) (Jain, 2009). VSL dating of sand-sized (63–90 μm) quartz from the Luochuan section generated ages up to ~900 ka, in agreement with independent age control (Ankjærgaard et al., 2016; Ankjærgaard, 2019). However, VSL dating of silt-sized (4–11 μm) quartz from the Luochuan section also showed the deviation of the natural and laboratory DRCs from ~250 Gy, which resulted in age underestimation for D_e values beyond 250 Gy (Rahimzadeh et al., 2021).

Compared to the OSL signal of quartz, the infrared stimulated luminescence (IRSL) from K-feldspar also saturates at a higher dose, which can increase the upper dating limit. However,

the application of IRSL dating with feldspar has been hampered by anomalous fading (Spooner, 1992; 1994). The thermally stable IRSL signal of K-feldspar still fades under ambient temperatures, due to quantum tunneling between the electron traps and holes (Wintle, 1973; Visocekas, 1985), which would result in age underestimation. Various fading correction methods have been proposed (Huntley and Lamothe, 2001; Lamothe, 2003; Huntley 2006; Kars et al., 2008). However, accurate fading-corrected ages rely both on the assumptions behind the fading correction models and accurate measurements of fading rates.

Thomsen et al. (2008) reported that the second-step IRSL signal measured at a higher temperature (225 °C) after a preceding IRSL measurement at 50 °C showed much less fading. Based on this observation, post-infrared infrared (pIRIR) dating protocols have been proposed, such as the two-step pIRIR protocols (Buylaert et al., 2009; Thiel et al., 2011; Reinmann and Tsukamoto, 2012) and the multiple-elevated-temperature (MET) pIRIR protocols (Li and Li, 2011; Fu and Li, 2013). An increasing number of studies have applied pIRIR dating to Chinese loess deposits older than the last glacial period (e.g., Buylaert et al., 2015; Stevens et al., 2018; Zhang et al., 2018; Wu et al., 2019). Specifically, long depositional hiatuses of up to ~60 kyr were identified by Stevens et al. (2018) at the Jingbian section on the northern margin of the CLP, and a depositional hiatus of ~30 kyr was also reported for the Zhenbeitai section, located at the boundary of the CLP and Mu Us desert (Wu et al., 2019).

(2) Details of the experiments and luminescence age model construction

Stainless steel tubes (diameter 5 cm, length 25 cm) were hammered into the newly-

excavated section of the Luochuan loess-paleosol sequence, and were then extracted, sealed and transported to the luminescence dating laboratory at the University of Hong Kong. In the laboratory, the samples were opened under subdued red light, and the outermost 2–3-cm of sample material from both ends of the tube was removed and used to measure the dose rate. The inner part of the sample was treated with 10 % HCl and 30 % H₂O₂ to remove carbonates and organic matter, respectively. The sample was then dried and sieved to separate the 63–90 µm grain size fraction. Heavy liquid separation was used to extract the K-feldspar grains (<2.58 g/cm³), which were then etched with 10 % HF, combined with magnetic stirring, for 5–15 min (depending on the abundance of the grains) to remove the surface layer affected by alpha irradiation (Duval et al., 2018). The etched K-feldspar grains were then mounted on 9.7-mm stainless steel discs (~3 mm in diameter) with silicone oil as an adhesive.

The MET-pIRIR signals of K-feldspar were measured in this study (Li and Li, 2011). D_e measurements were made using an automated Risø TL/OSL DA-20 reader, equipped with a ⁹⁰Sr/⁹⁰Y beta source (0.14 Gy/s on the stainless steel discs). Infrared light (870 ± 40 nm) was used for stimulation. Luminescence signals were detected by a photomultiplier tube with a filter pack comprising Schott BG–39 and Corning 7–59 filters. Both the SAR and MAR protocols were applied. For the SAR protocol, the preheat was performed at 300 °C for 60 s, and IR stimulations were successively carried out at temperatures of 50 °C, 100 °C, 150 °C, 200 °C and 250 °C for 100 s (Table S1). The initial 10 s signal of the decay curve was integrated, with the final 10 s signal subtracted as the background. The MET-pIRIR₂₅₀ signal was applied for SAR D_e estimation and age calculation. The signal intensities and the DRCs of the MET-

pIRIR₂₅₀ signal of two samples are shown in Fig. S1.

The MAR protocol was adopted from previous studies (Li et al., 2013; Chen et al., 2015). A cutheat treatment up to 500 °C was performed before administering the test dose to remove the ‘memory effect’ (Table S2). For the MAR protocol, all samples were preheated at 320 °C for 60 s, and then stimulated with IR light at 50 °C, 100 °C, 150 °C, 200 °C, 250 °C and 300 °C for 100 s (Table S2). The MET-pIRIR₃₀₀ signal was applied for MAR D_e estimation and age calculation. To directly compare the performances of SAR and MAR protocols, 9 samples from units S2–S3 were also measured with the preheat temperature at 320 °C and the highest pIRIR stimulation temperature at 300 °C. A comparison between the D_e values of different protocols is shown in Fig. S2.

Standard growth curves (SGCs) were constructed with the ‘regenerative-dose normalization’ method to reduce the measurement time of D_e (Li et al., 2015; Zhang and Li, 2019). For the SAR protocol, details of the SGC construction and D_e estimation were described in a previous study (Zhang and Li, 2019). For the MAR protocol, a new SGC was constructed in this study. The construction of the MAR SGC consisted of the following steps: 1) Aliquots of 13 samples were bleached using a solar simulator (ORIEL, with a 1000 W xenon arc lamp) for ~8 h. 2) The bleached aliquots of each sample were divided into several groups and given different regenerative doses (0–3000 Gy). Among them, a regenerative dose of 500 Gy was given to one group of aliquots for each sample. 3) For each sample, the sensitivity-corrected luminescence signal (L_x/T_x) of all the aliquots was normalized by the mean L_x/T_x value of the aliquots from the 500-Gy group. The test doses of all MAR measurements were fixed at 100

Gy. 4) The re-normalized L_x/T_x values of all the aliquots of all samples were plotted versus the corresponding regenerative doses, and the SGC was fitted with a single saturating exponential (SSE) and a double saturating exponential (DSE) function (Fig. S3). In this study, we applied the SSE function as it described the SGC quite well. The MAR SGC is: $y = 0.100 + 1.755 \cdot (1 - \exp(-x/695))$, where y is the re-normalized L_x/T_x , and x is the dose. The D_0 is 695 Gy.

After the MAR SGC was constructed, two groups of aliquots were prepared to measure D_e . One group of aliquots was used to measure the natural signal (L_n/T_n values), and the other group was bleached for ~8 h and then given a regenerative dose. The corresponding signals were then measured (L_x/T_x values). This regenerative dose (D_r) was generally set close to the expected D_e as it would provide greater accuracy for SGC D_e estimation (Li et al., 2015; Peng et al., 2016; Zhang and Li, 2019). The median value of the L_x/T_x values of the ‘regenerative-dose’ aliquots was used to re-normalize the median value of the L_n/T_n values of the ‘natural’ aliquots, as follows: $f(D_e) = f(D_r) \frac{L_n/T_n}{L_x/T_x}$, where $f(D_e)$ and $f(D_r)$ are the corresponding functional values of D_e and D_r in the MAR SGC. SGC D_e was calculated from $f(D_e)$. Median rather than mean values were used as the median values were less affected by the outliers. Outliers of the L_n/T_n or L_x/T_x values were identified and rejected by the median absolute deviation method using the criterion of 2.5 (Hu et al., 2019; Rousseeuw et al., 2006). The errors of the median L_n/T_n or L_x/T_x were calculated from the standard errors of all measured L_n/T_n or L_x/T_x values. D_e errors were calculated by error propagation.

To estimate the environmental dose rate, the contributions of U and Th were estimated using thick-source alpha counting. The counting rates were converted to β and γ dose rates

using conversion factors (Ademic and Aitken, 1998). Whole rock K concentrations were measured by X-ray fluorescence. The internal K and Rb concentrations of K-feldspar were assumed to be $13 \pm 1\%$ and 400 ± 100 ppm, respectively (Huntley and Baril, 1997; Zhao and Li, 2005). The cosmic-ray contribution was estimated according to the sampling altitude, latitude, and depth below the ground surface (Prescott and Hutton, 1994). Water contents were estimated based on previous studies. Lu et al. (2007) measured the in-situ water contents of units S0, L1 and S1 at the Luochuan section. Most samples from units L1-1 and L1-3 (MIS 2 and 4) had water contents of $15 \pm 2\%$, except for two samples adjacent to the L1-3/S1 boundary which had a water content of $25 \pm 2\%$. In unit L1-2 (MIS 3), the water contents of most samples were $20 \pm 2\%$ (Lu et al., 2007). In unit S1 (MIS 5), the water contents were $20\text{--}25 \pm 2\%$ (Lu et al., 2007). Here, we used water contents of $25 \pm 5\%$ for units S1, S2 and S3, and $15 \pm 5\%$ for units L2, L3 and L4. However, in the lower part of unit L2 (14.35–16.45 m), the water contents were set to $20 \pm 5\%$, as the lower part of unit L2 is close to unit L1-2 (MIS 3) in terms of the climate proxies. The four samples at the top of L2 (11.1–11.4 m in depth) have high carbonate concentrations (Fig. S4). The carbonate accumulation occurred long after the time of deposition, and the currently measured dose rates should be lower than the dose rates before carbonate accumulation (Zhang et al., 2018). Samples within the interval of 11.5–12.5 m were not subject to carbonate accumulation, and their mean dose rate (D_{r0}) may represent the initial dose rate of the four samples. For each of the four samples, a revised dose rate was calculated by taking the mean of its currently-measured dose rate and D_{r0} (Fig. S4). The revised ages were then used in Bacon age-depth modelling. The D_e values, dose rates and ages are summarized

in [Supplemental data.xlsx](#).

Numerous quartz OSL ages have already been reported for the Luochuan section (e.g., Lu et al., 2007, Lai, 2010; Fu et al., 2012). To correlate the sample depths, the S0/L1 and L1/S2 boundaries were used as tie points to adjust the depths in previous studies to the depths in our study. There is also a slight difference in the thickness of S0 and L1 between these studies. Once the boundary depths of S0 and L1 were fixed, the depths of samples within S0 and L1 were adjusted based on the relative position of each sample within S0 or L1. In this study, we used the 35 published quartz OSL ages (Lu et al., 2007, Lai, 2010; Fu et al., 2012), together with 96 feldspar pIRIR ages (50 SAR ages for samples above the L2/S2 boundary and 46 MAR ages for samples below the L2/S2 boundary). Bacon age-depth modelling was performed to obtain the absolute age model. Prior information about inverse accumulation rates consisting of a gamma distribution were set as: $\text{acc.shape} = 1.5$, and $\text{acc.mean} = 100\text{-}150$ years/cm for loess units and 300 years/cm for paleosol units. The prior acc.mean values were obtained from the linear fitting of depths and ages in each unit. Parameters for the memory effect consisting of a beta distribution were set as: $\text{mem.mean} = 0.7$ and $\text{mem.strength} = 4$, which were the same as in previous studies (Stevens et al., 2018). The modelling thickness was set as 10 cm and the modeled ages were also calculated at a resolution of 10 cm.

(3) Tests of the reliability of the dating protocols

a) Comparison of SAR and MAR D_e values

Generally, the MAR protocol generated D_e values larger than the SAR protocol. However, for the six samples above 16.5-m depth (i.e., the L2/S2 boundary), the mean age difference between the SAR and MAR was only 4 kyr. As the MAR ages used the pIRIR signal at 300 °C (MET-pIRIR₃₀₀) and the SAR ages used the pIRIR signal at 250 °C (MET-pIRIR₂₅₀), the slightly older MAR ages may be related to the higher residual dose and/or higher signal stability of the MET-pIRIR₃₀₀ signal compared to the MET-pIRIR₂₅₀ signal. However, an age difference of 4 kyr is negligible for the old samples used in this study. The SAR ages and MAR ages can still be regarded as consistent above the L2/S2 boundary. For the samples from unit S2, the SAR ages became systematically younger than the MAR ages. For samples below the S2/L3 boundary, the SAR ages ceased to increase with depth, while the MAR ages continued to increase with depth. The nine samples from units S2–S3 were repeatedly dated by the SAR protocol with a preheat temperature at 320 °C and the highest pIRIR stimulation temperature at 300 °C. The SAR D_e of the MET-pIRIR₃₀₀ signal was very close to the SAR D_e of the MET-pIRIR₂₅₀ signal, indicating that signal instability was not the cause of the SAR age underestimation here (Fig. S2). Instead, the underestimation is likely be related to the smaller D_0 in the DRC of the SAR protocol.

b) Residual dose

The pIRIR signal of K-feldspar measured at high temperatures may contain components that cannot be bleached by natural sunlight, which will result in age overestimation (Buylaert et al., 2011; Chen et al., 2013). To evaluate this influence of residual doses, several samples from units S1, L2 and S3 were bleached using a solar simulator (ORIEL, with a 1000 W xenon

arc lamp) for different intervals (1–8 h) and the residual doses were measured using the SAR protocol. The residual doses were < 8 Gy for the MET-pIRIR₂₅₀ signal and < 11 Gy for the MET-pIRIR₃₀₀ signal, after solar bleaching for 4 h (Fig. S5). Given that the D_e values adopted for establishing the luminescence age model were 300–700 Gy for the MET-pIRIR₂₅₀ signal (above L2/S2 boundary), and 700–1200 Gy for the MET-pIRIR₃₀₀ signal (below L2/S2 boundary), these residual doses have only negligible effects on the age estimation.

c) Signal stability

The proposal of the MET-pIRIR protocol is based on the assumption that when a D_e plateau is reached between pIRIR signals stimulated at high temperatures, these high temperature pIRIR signals can be regarded as stable signals with negligible fading (Li and Li, 2011; 2012). In this study, the D_e values of the pIRIR signals at 250 and 300 °C were consistent with each other, considering the errors (Fig. S6), which indicated the stability of the pIRIR signals at 250 °C and 300 °C. Additional evidence for signal stability is that our luminescence age model generated an age of 327 ± 14 ka for the S3/L4 boundary, with the MET-pIRIR₃₀₀ signal. Orbitally-tuned ages at this boundary between different studies are very similar to each other, within the range of 334–342 ka (Ding et al., 1994, 2002; Lu et al., 1999, 2022; Heslop et al., 2000; Sun et al., 2006a, b). The general consistency between our luminescence age model and the orbitally-tuned ages at this boundary indicates that the MET-pIRIR₃₀₀ signal has negligible fading for an age range up to ~ 350 ka. Thus, no fading correction was performed in this study.

d) Dose recovery tests

Dose recovery tests were performed to test the reliability of the protocols on the SAR D_e measurements. Several samples were bleached by the solar simulator for 2 h and then given different doses. Previous studies suggested that an appropriate test dose size should be used for successful dose recovery (Fu et al., 2015, Yi et al., 2016, Stevens et al., 2018). In this study, the SAR D_e values were measured using two different test doses, 72.5 Gy and 145 Gy, and dose recovery tests were also performed with these two test doses. The recovery ratios were calculated by dividing the measured doses (with the residual dose subtracted) by the given doses. Recovery ratios are plotted with the given doses in Fig. S7. With the test dose of 72.5 Gy, given doses of 200–550 Gy could be successfully recovered within 1.0 ± 0.1 . When the given doses were larger than 600 Gy, the recovered doses were overestimated by more than 10 %. With the test dose of 145 Gy, given doses of 300–750 Gy could be successfully recovered within 1.0 ± 0.1 . When the given doses were less than 300 Gy, the recovered doses were underestimated by more than 10 %. In this study, the test dose of 72.5 Gy was used for dating for samples with $D_e < 500$ Gy, and the test dose of 145 Gy was used for dating samples with $D_e > 500$ Gy, which always met the requirements for successful dose recovery.

For the MAR protocol, the pre-dose effect was completely removed by the ‘heat to 500 °C’ treatment and the test dose signals were only used for normalization between aliquots, as in mass normalization. The size of the test dose had no effect on the MAR D_e estimation. No dose recovery tests were performed for the MAR protocol. The consistency between the SAR and MAR ages in L2 unit also indicated the reliability of the MAR protocol.

(4) Global climatic evidence for reassigning the age of the MIS 8/9 boundary to ca. 280 ka

Much evidence suggests that the interglacial climate of MIS 9 continued to ca. 280 ka. The composite sea level record shows that the global sea level gradually decreased across the previous MIS 8/9 boundary (300 ka) but was followed by an increase in sea level which peaked at ca. 285 ka (Spratt and Lisiecki, 2016). This prolonged interglacial climate is also evident in key records from Eurasia, where the rainfall generally increased during interglacials. For example, on the CLP, unit S3 (corresponding to MIS 9) is a tricyclic paleosol at the Weinan loess section (Guo et al., 1996) and the Jingyuan section (Sun et al., 2006a). In semiarid central Asia, the stalagmite at Kesang Cave has three well-resolved $\delta^{18}\text{O}$ rainfall peaks, related to precession, during the period of 337–280 ka (Cheng et al., 2012). In southern Europe, there are three precessional cycles in arboreal pollen curves during MIS 9 (Tzedakis et al., 2001, 2006). These various lines of evidence suggest that it is more reasonable to reassign the age of the MIS 8/9 boundary from 300 ka to ca. 280 ka (Railsback et al., 2015).

Tables and Figures

Table S1. The SAR MET-pIRIR dating protocol used in this study (Li and Li, 2011).

| Step | Treatment | Observed |
|------|--------------------------------------|--------------|
| 1 | Give regenerative dose, D_i^a | |
| 2 | Preheat at 300 °C for 60 s | |
| 3 | IRSL measurement at 50 °C for 100 s | $L_{x(50)}$ |
| 4 | IRSL measurement at 100 °C for 100 s | $L_{x(100)}$ |
| 5 | IRSL measurement at 150 °C for 100 s | $L_{x(150)}$ |
| 6 | IRSL measurement at 200 °C for 100 s | $L_{x(200)}$ |
| 7 | IRSL measurement at 250 °C for 100 s | $L_{x(250)}$ |
| 8 | Give test dose, D_t | |
| 9 | Preheat at 300 °C for 60 s | |
| 10 | IRSL measurement at 50 °C for 100 s | $T_{x(50)}$ |
| 11 | IRSL measurement at 100 °C for 100 s | $T_{x(100)}$ |
| 12 | IRSL measurement at 150 °C for 100 s | $T_{x(150)}$ |
| 13 | IRSL measurement at 200 °C for 100 s | $T_{x(200)}$ |
| 14 | IRSL measurement at 250 °C for 100 s | $T_{x(250)}$ |
| 15 | IR bleaching at 320 °C for 100 s | |
| 16 | Return to step 1 | |

^a For the first cycle, D_i refers to the equivalent dose (D_e)

Table S2. The MAR MET-pIRIR dating protocol used in this study, modified from Li et al. (2013) and Chen et al. (2015).

| Step | Treatment | Observed |
|------|--------------------------------------|--------------|
| 1 | Give regenerative dose, D_i^a | |
| 2 | Preheat at 320 °C for 60 s | |
| 3 | IRSL measurement at 50 °C for 100 s | $L_{x(50)}$ |
| 4 | IRSL measurement at 100 °C for 100 s | $L_{x(100)}$ |
| 5 | IRSL measurement at 150 °C for 100 s | $L_{x(150)}$ |
| 6 | IRSL measurement at 200 °C for 100 s | $L_{x(200)}$ |
| 7 | IRSL measurement at 250 °C for 100 s | $L_{x(250)}$ |
| 8 | IRSL measurement at 300 °C for 100 s | $L_{x(300)}$ |
| 9 | Cutheat to 500 °C | |
| 10 | Give test dose, D_t | |
| 11 | Preheat at 320 °C for 60 s | |
| 12 | IRSL measurement at 50 °C for 100 s | $T_{x(50)}$ |
| 13 | IRSL measurement at 100 °C for 100 s | $T_{x(100)}$ |
| 14 | IRSL measurement at 150 °C for 100 s | $T_{x(150)}$ |
| 15 | IRSL measurement at 200 °C for 100 s | $T_{x(200)}$ |
| 16 | IRSL measurement at 250 °C for 100 s | $T_{x(250)}$ |
| 17 | IRSL measurement at 300 °C for 100 s | $L_{x(300)}$ |

^a For the first cycle, D_i refers to the equivalent dose (D_e)

Table S3. Boundary ages from the orbital-tuned timescales, Marine Isotope Stages, and the luminescence age model (Bacon age-depth modelled) built in this study.

| Boundary | Ding et al. (1994) (grain size) | Lu et al. (1999) (MS) | Heslop et al. (2000) (MS) | Ding et al. (2002) (grain size) | Sun et al. (2006a) (MS and grain size) | Sun et al. (2006b) (grain size) | Lu et al. (2022) (MS) | Lisiecki and Raymo (2005) (benthic $\delta^{18}\text{O}$) | This study, luminescence age model |
|----------|---------------------------------------|-----------------------------|---------------------------------|---------------------------------------|--|---------------------------------------|-----------------------------|--|------------------------------------|
| L1/S1 | 72 | 71 | 79 | 73 | 73 | 72 | 73 | 71 | 72 ± 3 |
| S1/L2 | 128 | 129 | 129 | 128 | 129 | 128 | 131 | 130 | 129 ± 4 |
| L2/S2 | 190 | 188 | 196 | 190 | 189 | 190 | 195 | 190 | 187 ± 7 |
| S2/L3 | 250 | 254 | 250 | 245 | 244 | 245 | 246 | 243 | 243 ± 8 |
| L3/S3 | 282 | 279 | 290 | 307 | 280 | 279 | 298 | 300 | 276 ± 9 |
| S3/L4 | 334 | 334 | 342 | 336 | 335 | 336 | 338 | 337 | 327 ± 14 |

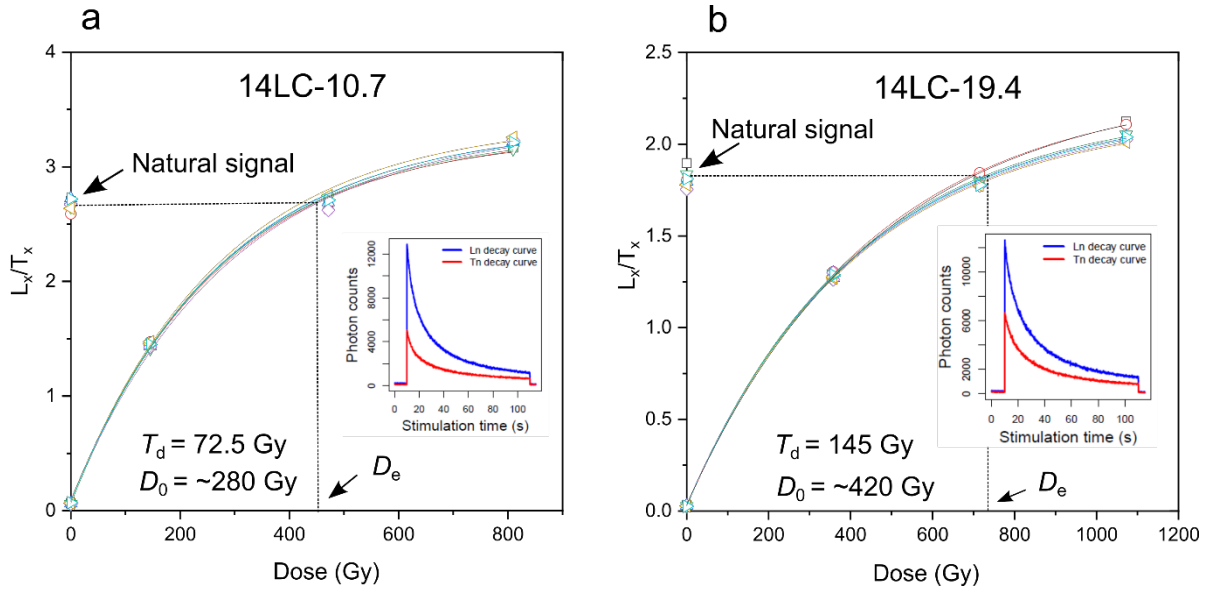


Figure S1. SAR D_e estimation from the dose response curves (DRCs) of samples 14LC-10.7 and 14LC-19.4, for the MET-pIRIR₂₅₀ signal. The DRCs were fitted with a single saturating exponential function: $y=y_0+a*(1-\exp(-x/D_0))$, where D_0 is the characteristic saturation dose. Data for seven aliquots for each sample are shown. Each symbol represents a single aliquot. The inset graphs illustrate the intensities of the natural signal and the test dose signal of a specific aliquot.

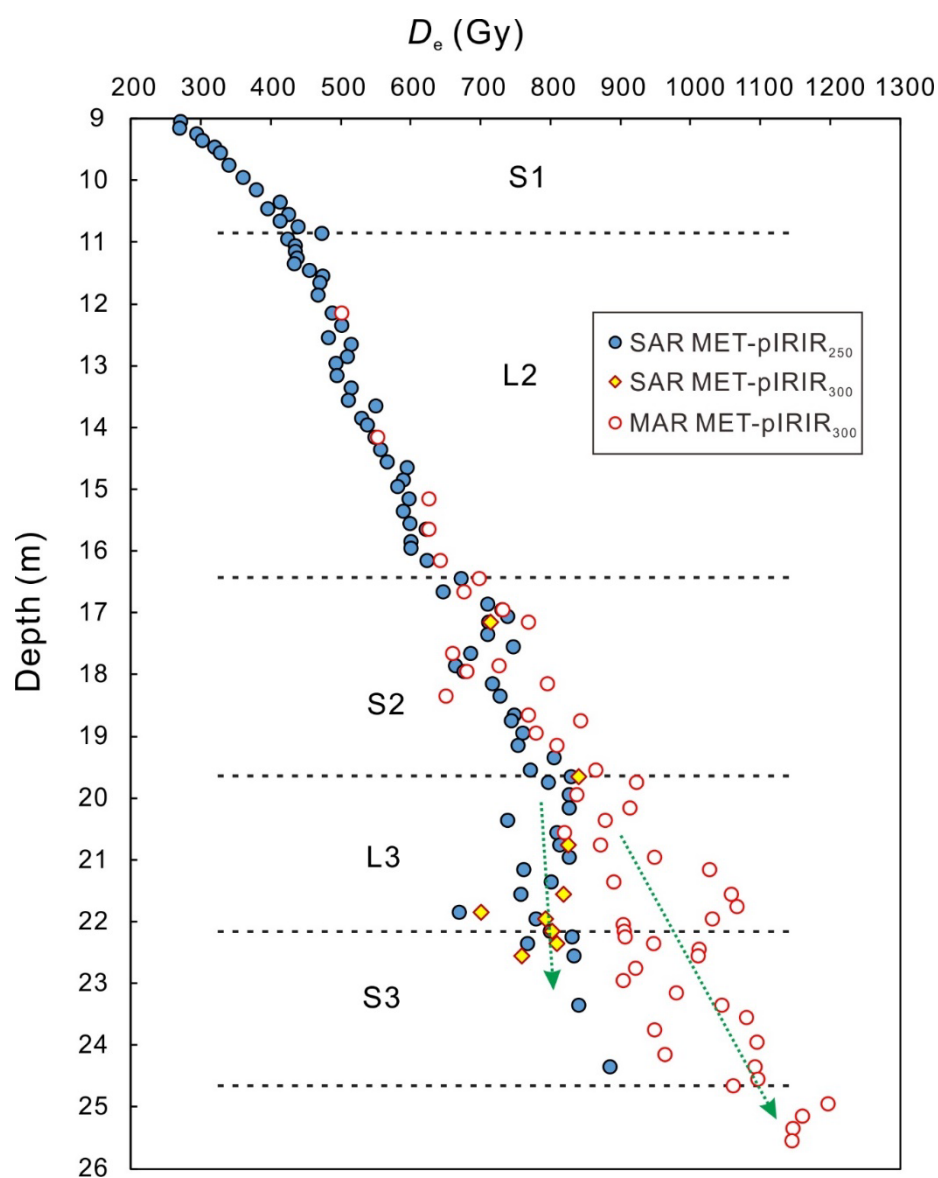


Figure S2. Comparison of SAR and MAR D_e values versus sampling depth. Note that the SAR D_e values become ‘saturated’ below S2. Detailed data are given in [Supplemental Data.xlsx](#).

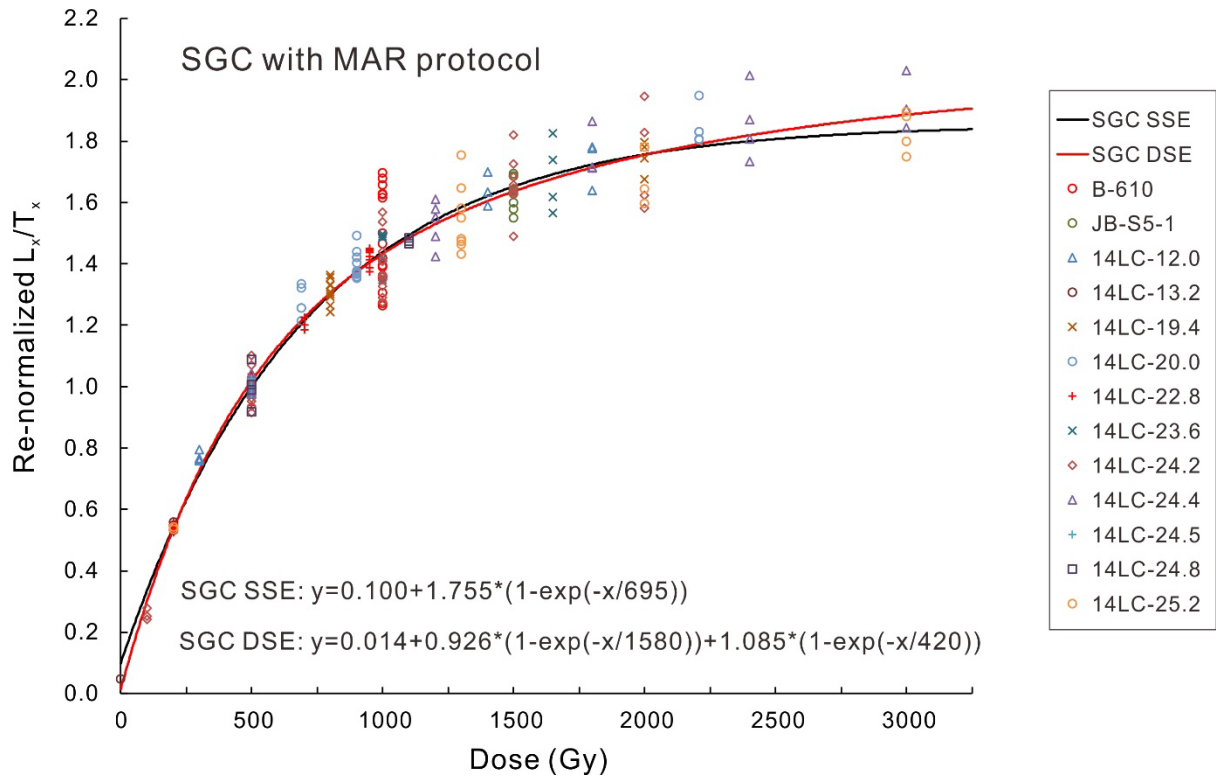


Figure S3. Standardized growth curves (SGCs) constructed for the MAR protocol, fitted with single saturating exponential (SSE) and double saturation exponential (DSE) functions. Note that the two SGCs are very similar when the dose is smaller than 2250 Gy. With the SSE fitting, D_0 is 695 Gy.

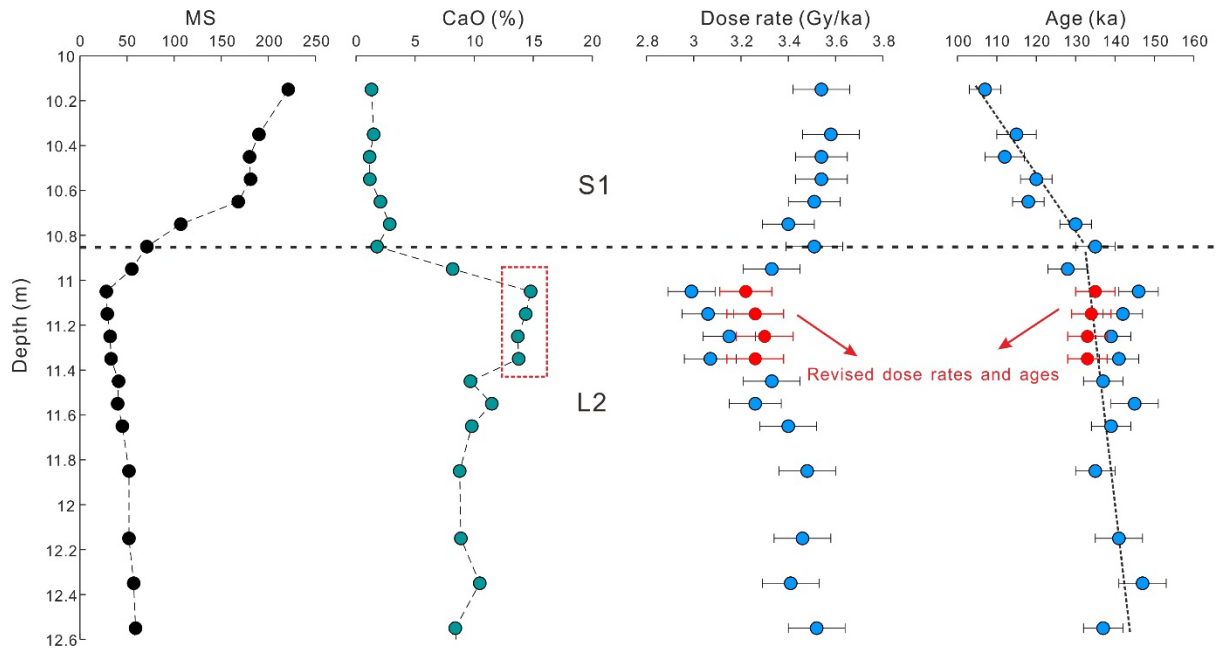


Figure S4. Dose rates and ages for samples at the S1/L2 boundary. The four samples at the top of L2 unit (11.1–11.4 m in depth) have high carbonate concentrations. Samples within the interval of 11.5–12.5 m were not affected by carbonate accumulation, and their mean dose rate was calculated to represent the initial dose rate of the four samples from the top of L2 (D_{r0}). For each of the four samples from the top of L2, a revised dose rate was calculated which is the mean of its currently measured dose rate and D_{r0} . The red data points represent the revised dose rates and ages of the four samples. The revised ages were used in Bacon age-depth modelling.

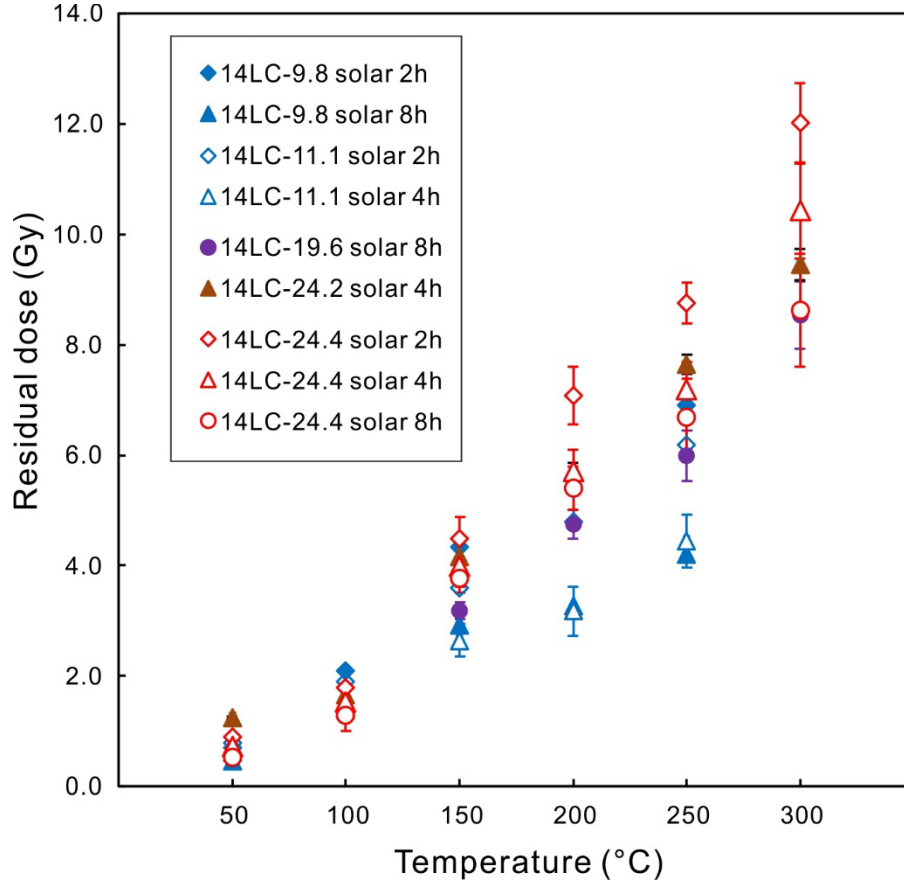


Figure S5. Residual doses of IR or pIRIR signals at different temperatures, measured after different durations of solar simulator bleaching. Each data point is an average of 2–3 aliquots and the error bar refers to one standard error. After solar bleaching for 4 h, the residual doses were < 8 Gy for the MET-pIRIR₂₅₀ signal and < 11 Gy for the MET-pIRIR₃₀₀ signal.

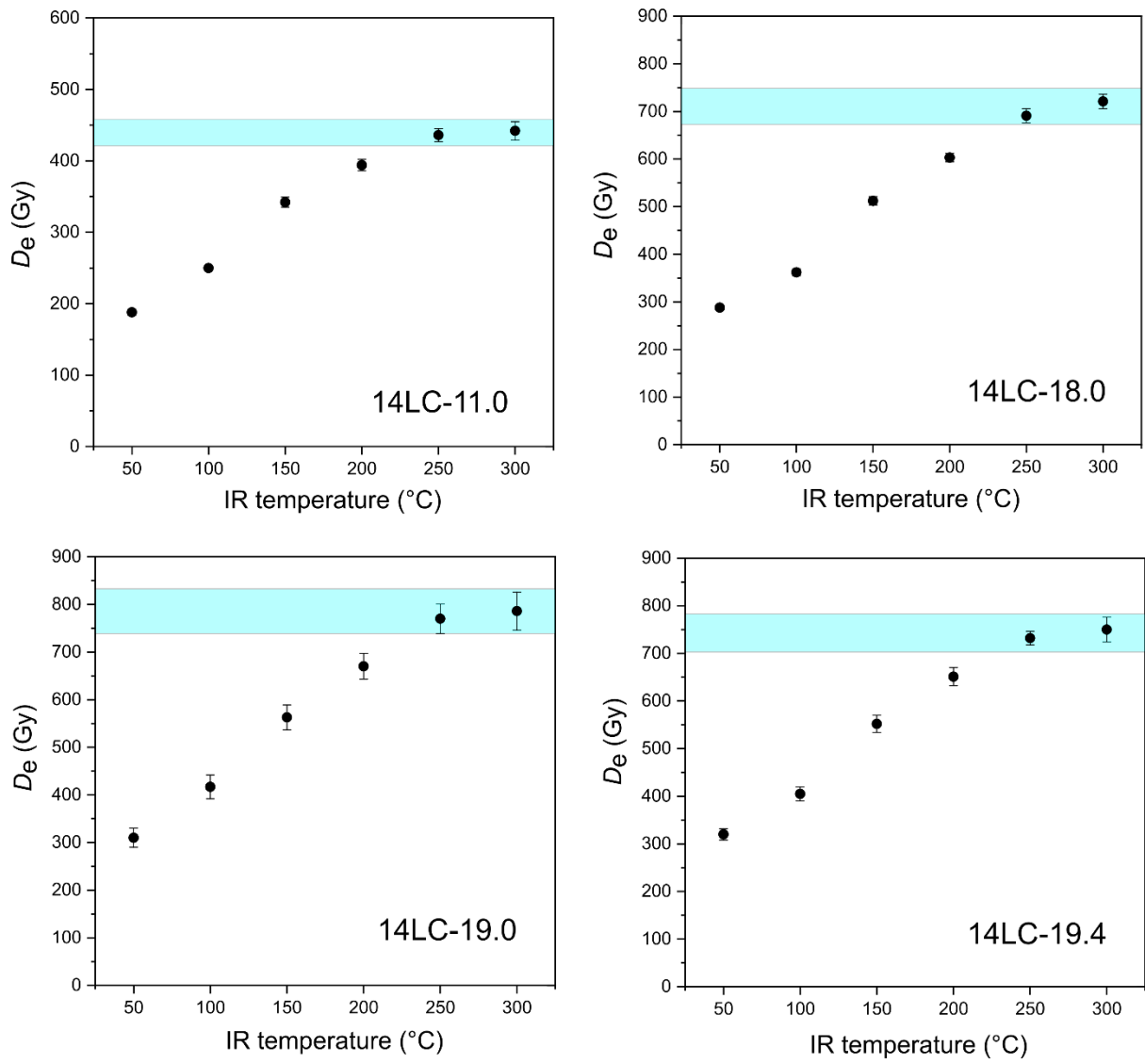


Figure S6. SAR D_e versus IR and pIRIR signals at different stimulation temperatures. D_e values are close to each other for pIRIR signals at 250 °C and 300 °C, which indicates that the fading of these signals measured at 250 °C and 300 °C is negligible.

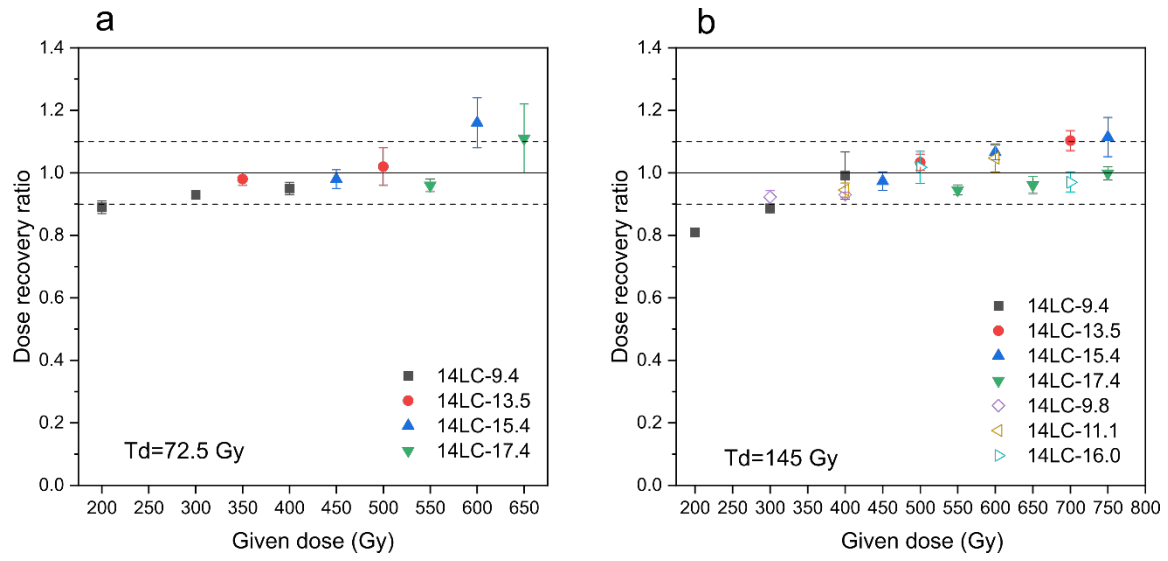


Figure S7. Dose recovery results with two different test doses (T_d). With a test dose of 72.5 Gy, given doses within the range of 200–550 Gy were successfully recovered (within 1.0 ± 0.1). With a test dose of 145 Gy, given doses within the range of 300–750 Gy were successfully recovered.

References

- Ademic, G., and Aitken, M. J., 1998, Dose-rate conversion factors: update: *Ancient TL*, v. 16, p. 37–50.
- Ankjærgaard, C., 2019, Exploring multiple-aliquot methods for quartz violet stimulated luminescence dating: *Quaternary Geochronology*, v. 51, p. 99–109.
- Ankjærgaard, C., Guralnik, B., Buylaert, J. P., Reimann, T., Yi, S. W., and Wallinga, J., 2016, Violet stimulated luminescence dating of quartz from Luochuan (Chinese loess plateau): Agreement with independent chronology up to ~600 ka: *Quaternary Geochronology*, v. 34, p. 33–46.
- Buylaert, J. P., Murray, A. S., Vandenberghe, D., Vriend, M., De Corte, F., and Van den haute, P., 2008, Optical dating of Chinese loess using sand-sized quartz: Establishing a time frame for Late Pleistocene climate changes in the western part of the Chinese Loess Plateau: *Quaternary Geochronology*, v. 3, no. 1-2, p. 99–113.
- Buylaert, J.P., Murray, A.S., Thomsen, K.J., and Jain, M., 2009, Testing the potential of an elevated temperature IRSL signal from K-feldspar: *Radiation Measurements*, v. 44, p. 560–565.
- Buylaert, J.-P., Thiel, C., Murray, A., Vandenberghe, D., Yi, S., and Lu, H., 2011, IRSL and post-IR IRSL residual doses recorded in modern dust samples from the Chinese Loess Plateau: *Geochronometria*, v. 38, p. 432–440.
- Buylaert, J.P., Vandenberghe, D., Murray, A.S., Huot, S., Corte, F.D., and Haute, P.V. den, 2007, Luminescence dating of old (>70ka) Chinese loess: A comparison of single-aliquot OSL and IRSL techniques: *Quaternary Geochronology*, v. 2, p. 9–14.
- Buylaert, J.-P., Yeo, E.-Y., Thiel, C., Yi, S., Stevens, T., Thompson, W., Frechen, M., Murray, A., and Lu, H., 2015, A detailed post-IR IRSL chronology for the last interglacial soil at the Jingbian loess site (northern China): *Quaternary Geochronology*, v. 30, p. 194–199.
- Chapot, M. S., Roberts, H. M., Duller, G. A. T., and Lai, Z. P., 2012, A comparison of natural- and laboratory-generated dose response curves for quartz optically stimulated luminescence signals from Chinese Loess: *Radiation Measurements*, v. 47, no. 11, p. 1045–1052.
- Chapot, M. S., Roberts, H. M., Duller, G. A. T., and Lai, Z. P., 2016, Natural and laboratory TT-OSL dose response curves: Testing the lifetime of the TT-OSL signal in nature: *Radiation Measurements*, v. 85, p. 41–50.
- Chen, Y., Li, S.-H., and Li, B., 2013, Residual doses and sensitivity change of post IR IRSL signals from potassium feldspar under different bleaching conditions: *Geochronometria*, v. 40, p. 229–238.
- Chen, Y. W., Li, S. H., Li, B., Hao, Q. Z., and Sun, J. M., 2015, Maximum age limitation in luminescence dating of Chinese loess using the multiple-aliquot MET-pIRIR signals from K-feldspar: *Quaternary Geochronology*, v. 30, p. 207–212.
- Cheng, H., Zhang, P. Z., Spotl, C., Edwards, R. L., Cai, Y. J., Zhang, D. Z., Sang, W. C., Tan, M., and An, Z. S., 2012, The climatic cyclicity in semiarid-arid central Asia over the past

-
- 500,000 years: *Geophysical Research Letters*, v. 39.
- Ding, Z., Yu, Z., Rutter, N. W., and Liu, T., 1994, Towards an Orbital Time-Scale for Chinese Loess Deposits: *Quaternary Science Reviews*, v. 13, no. 1, p. 39–70.
- Ding, Z. L., Derbyshire, E., Yang, S. L., Yu, Z. W., Xiong, S. F., and Liu, T. S., 2002, Stacked 2.6-Ma grain size record from the Chinese loess based on five sections and correlation with the deep-sea delta O-18 record: *Paleoceanography*, v. 17, no. 3.
- Duval, M., Guilarte, V., Campaña, I., Arnold L.J., Miguens, L., Iglesias, J., and González-Sierra, S. 2018. Quantifying hydrofluoric acid etching of quartz and feldspar coarse grains based on weight loss estimates: implication for ESR and luminescence dating studies. *Ancient TL*, v. 36 (1), p. 1–14.
- Fan, A., Li, S.-H., and Li, B., 2011, Observation of unstable fast component in OSL of quartz: *Radiation Measurements*, v. 46, no. 1, p. 21–28.
- Fu, X., and Li, S.-H., 2013, A modified multi-elevated-temperature post-IR IRSL protocol for dating Holocene sediments using K-feldspar: *Quaternary Geochronology*, v. 17, p. 44–54.
- Fu, X., Li, B., and Li, S. H., 2012, Testing a multi-step post-IR IRSL dating method using polymineral fine grains from Chinese loess: *Quaternary Geochronology*, v. 10, p. 8–15.
- Fu, X., Li, S. H., and Li, B., 2015, Optical dating of aeolian and fluvial sediments in north Tian Shan range, China: Luminescence characteristics and methodological aspects: *Quaternary Geochronology*, v. 30, p. 161–167.
- Guo, Z. T., Ding, Z. L., and Liu, T. S., 1996, Pedosedimentary events in loess of China and Quaternary climatic cycles: *Chinese Science Bulletin*, v. 41, no. 14, p. 1189–1193.
- Heslop, D., Langereis, C. G., and Dekkers, M. J., 2000, A new astronomical timescale for the loess deposits of Northern China: *Earth and Planetary Science Letters*, v. 184, no. 1, p. 125–139.
- Hu, Y., Marwick, B., Zhang, J.-F., Rui, X., Hou, Y.-M., Yue, J.-P., Chen, W.-R., Huang, W.-W., and Li, B., 2019, Late Middle Pleistocene Levallois stone-tool technology in southwest China: *Nature*, v. 565, no. 7737, p. 82–85.
- Huntley, D.J., 2006, An explanation of the power-law decay of luminescence: *Journal of Physics: Condensed Matter*, v. 18, p. 1359–1365.
- Huntley, D. J., and Baril, M. R., 1997, The K content of the K-feldspars being measured in optical dating or in thermoluminescence dating: *Ancient TL*, v. 15, p. 11–13.
- Huntley, D. J., and Lamothe, M., 2001, Ubiquity of anomalous fading in K-feldspars and the measurement and correction for it in optical dating: *Canadian Journal of Earth Sciences*, v. 38, no. 7, p. 1093–1106.
- Jain, M., 2009, Extending the dose range: Probing deep traps in quartz with 3.06eV photons: *Radiation Measurements*, v. 44, no. 5, p. 445–452.
- Kang, S., Du, J., Wang, N., Dong, J., Wang, D., Wang, X., Qiang, X., and Song, Y., 2020, Early Holocene weakening and mid-to late Holocene strengthening of the East Asian winter monsoon: *Geology*, v. 48, p. 1043–1047.
- Kang, S., Lu, Y., and Wang, X., 2011, Closely-spaced recuperated OSL dating of the last interglacial paleosol in the southeastern margin of the Chinese Loess Plateau: *Quaternary*

-
- Geochronology, v. 6, p. 480–490.
- Kang, S., Roberts, H.M., Wang, X., An, Z., and Wang, M., 2015, Mass accumulation rate changes in Chinese loess during MIS 2, and asynchrony with records from Greenland ice cores and North Pacific Ocean sediments during the Last Glacial Maximum: *Aeolian Research*, v. 19, p. 251–258.
- Kang, S. G., Wang, X. L., and Lu, Y. C., 2013, Quartz OSL chronology and dust accumulation rate changes since the Last Glacial at Weinan on the southeastern Chinese Loess Plateau: *Boreas*, v. 42, no. 4, p. 815–829.
- Kang, S., Wang, X., Roberts, H. M., Duller, G. A. T., Cheng, P., Lu, Y., and An, Z., 2018, Late Holocene anti-phase change in the East Asian summer and winter monsoons: *Quaternary Science Reviews*, v. 188, p. 28–36.
- Kars, R. H., Wallinga, J., and Cohen, K. M., 2008, A new approach towards anomalous fading correction for feldspar IRSL dating - tests on samples in field saturation: *Radiation Measurements*, v. 43, no. 2-6, p. 786–790.
- Lai, Z. P., 2010, Chronology and the upper dating limit for loess samples from Luochuan section in the Chinese Loess Plateau using quartz OSL SAR protocol: *Journal of Asian Earth Sciences*, v. 37, no. 2, p. 176–185.
- Lai, Z. P., and Fan, A. C., 2014, Examining quartz OSL age underestimation for loess samples from Luochuan in the Chinese Loess Plateau: *Geochronometria*, v. 41, no. 1, p. 57–64.
- Lai, Z. P., and Wintle, A. G., 2006, Locating the boundary between the Pleistocene and the Holocene in Chinese loess using luminescence: *Holocene*, v. 16, no. 6, p. 893–899.
- Lai, Z. P., Wintle, A. G., and Thomas, D. S. G., 2007, Rates of dust deposition between 50 ka and 20 ka revealed by OSL dating at Yuanbao on the Chinese Loess Plateau: *Palaeogeography Palaeoclimatology Palaeoecology*, v. 248, no. 3–4, p. 431–439.
- Lamothe, M., Auclair, M., Hamzaoui, C., and Huot, S., 2003, Towards a prediction of long-term anomalous fading of feldspar IRSL: *Radiation Measurements*, v. 37, no. 4–5, p. 493–498.
- Li, B., and Li, S.-H., 2011, Luminescence dating of K-feldspar from sediments: A protocol without anomalous fading correction: *Quaternary Geochronology*, v. 6, no. 5, p. 468–479.
- Li, B., and Li, S.-H., 2012, Luminescence dating of Chinese loess beyond 130 ka using the non-fading signal from K-feldspar: *Quaternary Geochronology*, v. 10, p. 24–31.
- Li, B., Jacobs, Z., Roberts, R. G., and Li, S. H., 2013, Extending the age limit of luminescence dating using the dose-dependent sensitivity of MET-pIRIR signals from K-feldspar: *Quaternary Geochronology*, v. 17, p. 55–67.
- Li, B., Roberts, R. G., Jacobs, Z., Li, S. H., and Guo, Y. J., 2015, Construction of a 'global standardised growth curve' (gSGC) for infrared stimulated luminescence dating of K-feldspar: *Quaternary Geochronology*, v. 27, p. 119–130.
- Lisiecki, L. E., and Raymo, M. E., 2005, A Pliocene-Pleistocene stack of 57 globally distributed benthic delta O-18 records: *Paleoceanography*, v. 20, no. 1.
- Liu, J., Murray, A. S., Buylaert, J. P., Jain, M., Chen, J., and Lu, Y. J. B., 2016, Stability of fine-grained TT-OSL and post-IR IRSL signals from a *c.* 1 Ma sequence of aeolian and

-
- lacustrine deposits from the Nihewan Basin (northern China), v. 45, no. 4, p. 703–714.
- Lu, H., Liu, X. D., Zhang, F. Q., An, Z. S., and Dodson, J., 1999, Astronomical calibration of loess-paleosol deposits at Luochuan, central Chinese Loess Plateau: *Palaeogeography Palaeoclimatology Palaeoecology*, v. 154, no. 3, p. 237–246.
- Lu, H., Stevens, T., Yi, S. W., and Sun, X. F., 2006, An erosional hiatus in Chinese loess sequences revealed by closely spaced optical dating: *Chinese Science Bulletin*, v. 51, no. 18, p. 2253–2259.
- Lu, H., Wang, X., Wang, Y., Zhang, X., Yi, S., Wang, X., Stevens, T., Kurbanov, R., and Marković, S. B., 2022, Chinese loess and the Asian monsoon: What we know and what remains unknown: *Quaternary International*, v. 620, p. 85–97.
- Lu, H., Yi, S., Liu, Z., Mason, J.A., Jiang, D., Cheng, J., Stevens, T., Xu, Z., Zhang, E., and Jin, L., 2013, Variation of East Asian monsoon precipitation during the past 21 ky and potential CO₂ forcing. *Geology* v.41, p. 1023–1026.
- Lu, Y. C., Wang, X. L., and Wintle, A. G., 2007, A new OSL chronology for dust accumulation in the last 130,000 yr for the Chinese Loess Plateau: *Quaternary Research*, v. 67, no. 1, p. 152–160.
- Murray, A. S., and Wintle, A. G., 2000, Luminescence dating of quartz using an improved single-aliquot regenerative-dose protocol: *Radiation Measurements*, v. 32, no. 1, p. 57–73.
- Perić, Z., Lagerbäck Adolphi, E., Stevens, T., Újvári, G., Zeeden, C., Buylaert, J.-P., Marković, S. B., Hambach, U., Fischer, P., Schmidt, C., Schulte, P., Huayu, L., Shuangwen, Y., Lehmkuhl, F., Obrecht, I., Veres, D., Thiel, C., Frechen, M., Jain, M., Vött, A., Zöller, L., and Gavrilov, M. B., 2019, Quartz OSL dating of late quaternary Chinese and Serbian loess: A cross Eurasian comparison of dust mass accumulation rates: *Quaternary International*, v. 502, p. 30–44.
- Prescott, J. R., and Hutton, J. T., 1994, Cosmic-Ray Contributions to Dose-Rates for Luminescence and ESR Dating - Large Depths and Long-Term Time Variations: *Radiation Measurements*, v. 23, no. 2-3, p. 497–500.
- Railsback, L. B., Gibbard, P. L., Head, M. J., Voarintsoa, N. R. G., and Toucanne, S., 2015, An optimized scheme of lettered marine isotope substages for the last 1.0 million years, and the climatostratigraphic nature of isotope stages and substages: *Quaternary Science Reviews*, v. 111, p. 94–106.
- Rousseeuw, P. J., Debruyne, M., Engelen, S., and Hubert, M., 2006, Robustness and outlier detection in chemometrics: *Critical Reviews in Analytical Chemistry*, v. 36, no. 3–4, p. 221–242.
- Rahimzadeh, N., Tsukamoto, S., Zhang, J., and Long, H., 2021, Natural and laboratory dose response curves of quartz violet stimulated luminescence (VSL): Exploring the multiple aliquot regenerative dose (MAR) protocol: *Quaternary Geochronology*, v. 65, p. 101194.
- Reimann, T., and Tsukamoto, S., 2012, Dating the recent past (<500 years) by post-IR IRSL feldspar – Examples from the North Sea and Baltic Sea coast: *Quaternary Geochronology*, v. 10, p. 180–187.
- Spratt, R. M., and Lisiecki, L. E., 2016, A Late Pleistocene sea level stack: *Climate of the Past*,

-
- v. 12, no. 4, p. 1079–1092.
- Spooner, N. A., 1992, Optical dating: Preliminary results on the anomalous fading of luminescence from feldspars: *Quaternary Science Reviews*, v. 11, no. 1–2, p. 139–145.
- Spooner, N. A., 1994, The Anomalous Fading of Infrared-Stimulated Luminescence from Feldspars: *Radiation Measurements*, v. 23, no. 2–3, p. 625–632.
- Stevens, T., Armitage, S. J., Lu, H. Y., and Thomas, D. S. G., 2006, Sedimentation and diagenesis of Chinese loess: Implications for the preservation of continuous, high-resolution climate records: *Geology*, v. 34, no. 10, p. 849–852.
- Stevens, T., Adamiec, G., Bird, A. F., and Lu, H. Y., 2013, An abrupt shift in dust source on the Chinese Loess Plateau revealed through high sampling resolution OSL dating: *Quaternary Science Reviews*, v. 82, p. 121–132.
- Stevens, T., Buylaert, J. P., Thiel, C., Ujvari, G., Yi, S., Murray, A. S., Frechen, M., and Lu, H., 2018, Ice-volume-forced erosion of the Chinese Loess Plateau global Quaternary stratotype site: *Nature Communications*, v. 9.
- Stevens, T., Lu, H. Y., Thomas, D. S. G., and Armitage, S. J., 2008, Optical dating of abrupt shifts in the late Pleistocene East Asian monsoon: *Geology*, v. 36, no. 5, p. 415–418.
- Stevens, T., Thomas, D.S.G., Armitage, S.J., Lunn, H.R., and Lu, H., 2007, Reinterpreting climate proxy records from late Quaternary Chinese loess: A detailed OSL investigation: *Earth-Science Reviews*, v. 80, p. 111–136.
- Sun, Y.B., Chen, J., Clemens, S. C., Liu, Q. S., Ji, J. F., and Tada, R., 2006a, East Asian monsoon variability over the last seven glacial cycles recorded by a loess sequence from the northwestern Chinese Loess Plateau: *Geochemistry Geophysics Geosystems*, v. 7.
- Sun, Y. B., Clemens, S. C., An, Z. S., and Yu, Z. W., 2006b, Astronomical timescale and palaeoclimatic implication of stacked 3.6-Myr monsoon records from the Chinese Loess Plateau: *Quaternary Science Reviews*, v. 25, no. 1–2, p. 33–48.
- Sun, Y. B., Clemens, S. C., Morrill, C., Lin, X. P., Wang, X. L., and An, Z. S., 2012, Influence of Atlantic meridional overturning circulation on the East Asian winter monsoon: *Nature Geoscience*, v. 5, no. 1, p. 46–49.
- Sun, Y. B., Wang, X. L., Liu, Q. S., and Clemens, S. C., 2010, Impacts of post-depositional processes on rapid monsoon signals recorded by the last glacial loess deposits of northern China: *Earth and Planetary Science Letters*, v. 289, no. 1–2, p. 171–179.
- Thiel, C., Buylaert, J.-P., Murray, A., Terhorst, B., Hofer, I., Tsukamoto, S., and Frechen, M., 2011, Luminescence dating of the Stratzing loess profile (Austria) – Testing the potential of an elevated temperature post-IR IRSL protocol: *Quaternary International*, v. 234, p. 23–31.
- Thomsen, K. J., Murray, A. S., Jain, M., and Botter-Jensen, L., 2008, Laboratory fading rates of various luminescence signals from feldspar-rich sediment extracts: *Radiation Measurements*, v. 43, no. 9–10, p. 1474–1486.
- Timar-Gabor, A., and Wintle, A. G., 2013, On natural and laboratory generated dose response curves for quartz of different grain sizes from Romanian loess: *Quaternary Geochronology*, v. 18, p. 34–40.

-
- Timar-Gabor, A., Buylaert, J. P., Guralnik, B., Trandafir-Antohei, O., Constantin, D., Anechitei-Deacu, V., Jain, M., Murray, A. S., Porat, N., Hao, Q., and Wintle, A. G., 2017, On the importance of grain size in luminescence dating using quartz: *Radiation Measurements*, v. 106, p. 464–471.
- Timar-Gabor, A., Constantin, D., Buylaert, J. P., Jain, M., Murray, A. S., and Wintle, A. G., 2015, Fundamental investigations of natural and laboratory generated SAR dose response curves for quartz OSL in the high dose range: *Radiation Measurements*, v. 81, p. 150–156.
- Tzedakis, P. C., Andrieu, V., de Beaulieu, J. L., Birks, H. J. B., Crowhurst, S., Follieri, M., Hooghiemstra, H., Magri, D., Reille, M., Sadori, L., Shackleton, N. J., and Wijmstra, T. A., 2001, Establishing a terrestrial chronological framework as a basis for biostratigraphical comparisons: *Quaternary Science Reviews*, v. 20, no. 16–17, p. 1583–1592.
- Tzedakis, P. C., Hooghiemstra, H., and Pälike, H., 2006, The last 1.35 million years at Tenaghi Philippon: revised chronostratigraphy and long-term vegetation trends: *Quaternary Science Reviews*, v. 25, no. 23–24, p. 3416–3430.
- Visocekas, R., 1985, Tunneling Radiative Recombination in Labradorite - Its Association with Anomalous Fading of Thermo-Luminescence: *Nuclear Tracks and Radiation Measurements*, v. 10, no. 4–6, p. 521–529.
- Wang, X.L., Lu, Y.C., and Wintle, A.G., 2006, Recuperated OSL dating of fine-grained quartz in Chinese loess: *Quaternary Geochronology*, v. 1, p. 89–100.
- Wintle, A. G., 1973, Anomalous Fading of Thermoluminescence in Mineral Samples: *Nature*, v. 245, no. 5421, p. 143–144.
- Wintle, A. G., and Murray, A. S., 2006, A review of quartz optically stimulated luminescence characteristics and their relevance in single-aliquot regeneration dating protocols: *Radiation Measurements*, v. 41, no. 4, p. 369–391.
- Wu, J., Lu, H., Yi, S., Xu, Z., Gu, Y., Liang, C., Cui, M., and Sun, X., 2019, Establishing a high-resolution luminescence chronology for the Zhenbeitai sand-loess section at Yulin, North-Central China: *Quaternary Geochronology*, v. 49, p. 78–84.
- Yi, S. W., Buylaert, J. P., Murray, A. S., Lu, H. Y., Thiel, C., and Zeng, L., 2016, A detailed post-IR IRSL dating study of the Niuyangzigou loess site in northeastern China: *Boreas*, v. 45, no. 4, p. 644–657.
- Zhang, J. J., and Li, S. H., 2019, Constructions of standardised growth curves (SGCs) for IRSL signals from K-feldspar, plagioclase and polymineral fractions: *Quaternary Geochronology*, v. 49, p. 8–15.
- Zhang, J. J., Li, S. H., Sun, J. M., and Hao, Q. Z., 2018, Fake age hiatus in a loess section revealed by OSL dating of calcrete nodules: *Journal of Asian Earth Sciences*, v. 155, p. 139–145.
- Zhao, H., and Li, S. H., 2005, Internal dose rate to K-feldspar grains from radioactive elements other than potassium: *Radiation Measurements*, v. 40, no. 1, p. 84–93.